Solid-Phase Epitaxy of Perovskite High Dielectric $PrAlO_3$ Films Grown by Atomic Layer Deposition for Use in Two-Dimensional Electronics and Memory Devices

Wathsala L. I. Waduge,[†] Yajin Chen,[‡] Peng Zuo,[‡] Navoda Jayakodiarachchi,[†] Thomas F. Kuech,[§] Susan E. Babcock,[‡] Paul G. Evans,[‡] and Charles H. Winter[,†]*

[†]Department of Chemistry, Wayne State University, Detroit, Michigan 48202

[‡]Department of Materials Science and Engineering, University of Wisconsin-Madison, Madison, Wisconsin 53706

[§]Department of Chemical and Biological Engineering, University of Wisconsin-Madison, Madison, Wisconsin 53706

KEYWORDS. Praseodymium aluminum oxide, atomic layer deposition, solid phase epitaxy, epitaxial film growth.

ABSTRACT. An atomic layer deposition (ALD) process is reported for the growth of nanoscale $PrAlO_3$ thin films for two-dimensional electronics and memory device applications using tris(isopropylcyclopentadienyl)praseodymium ($Pr(C_5H_4iPr)_3$), trimethylaluminum ($AlMe_3$), and water. $Pr(C_5H_4iPr)_3$ was first evaluated as a precursor for the formation of thin films of the binary oxide Pr_2O_3 using water as the co-reactant. Self-limited growth of Pr_2O_3 was demonstrated for pulse lengths of ≥3 s, with a growth rate of ~0.85 Å/cycle. The ALD growth of $PrAlO_3$ films was examined on Si, thermal SiO_2, and (001)-oriented $SrTiO_3$ substrates. Self-limited growth was demonstrated for $Pr(C_5H_4iPr)_3$, $AlMe_3$, and water at 300 °C using a 1:1 ratio of the number of $Pr(C_5H_4iPr)_3$ and $AlMe_3$ pulses. An ALD window was observed from 275 to 325 °C with a growth rate of ~1.7 Å/cycle. The as-deposited $PrAlO_3$ films on all substrates were amorphous, had smooth surfaces, and contained <0.5% carbon, as analyzed by grazing incidence wide-angle X-ray scattering, X-ray reflectivity, and X-ray photoelectron spectroscopy, respectively. Films grown with a 1:1 ratio of $Pr(C_5H_4iPr)_3$ and $AlMe_3$ pulses were aluminum-rich (Pr:Al ~1:1.2-1.4). Heating $PrAlO_3$ layers deposited on $SrTiO_3$ to 800 °C for 3 h resulted in fully crystallized $PrAlO_3$ films. The crystallized $PrAlO_3$ films were highly (001)-oriented. The $PrAlO_3$ 00L and $SrTiO_3$ 00L reflections appeared on the same rod of reciprocal space, further indicating that the amorphous $PrAlO_3$ film transforms into an epitaxial layer. The rocking curve width of the $PrAlO_3$ (001) reflection was 7°. By contrast, $PrAlO_3$ films deposited on Si substrates with native oxide remained amorphous after annealing at 1000 °C for 8 h. The difference in the crystallization between $PrAlO_3$ layers deposited on crystalline $SrTiO_3$ and amorphous native SiO_2 substrates indicates that $PrAlO_3$ on $SrTiO_3$ crystallized by solid phase epitaxy, in which the nucleation and orientation of the crystallized layer are set by the atomic configuration at the substrate-film interface.

INTRODUCTION

Binary early lanthanide oxides and ternary analogs containing aluminum and other metals are of significant interest for applications as future high-dielectric-constant materials in transistors and memory devices.[1-7] Ternary oxides such as $LaAlO_3$, $PrAlO_3$, and $NdAlO_3$ deposited on $SrTiO_3$ substrates are also important because of their interfacial two-dimensional electron gas properties.[8-14] Use of lanthanide oxides in practical applications requires their controlled growth as thin films, which has largely been accomplished to date using methods that allow the creation of planar two-dimensional thin films, but which are in fact also limited to these geometries. The development of novel deposition and crystallization methods has the potential to expand the scope of electronic applications of lanthanide aluminate materials by increasing the range of available substrates beyond those available with deposition techniques such as pulsed-laser deposition, molecular beam epitaxy, metalorganic chemical vapor deposition, and others.[15-17] Additional applications will arise if lanthanide aluminates can be crystallized in three-dimensional geometries beyond planar thin films.[18]

The lanthanide aluminates are significantly more stable chemically than the lanthanide oxides. Early lanthanide oxides react with water to form lanthanide hydroxide phases and ambient CO_2 to form carbonates.[1,19-21] These reactions create problems for applications of early lanthanide oxide films, since water and CO_2 can complicate depositions and the resulting films are unstable in air. However, incorporation of aluminum oxides stabilizes the resulting $LnAlO_3$ (Ln = lanthanide) phases against reaction with water and CO_2, since the alumina-based layers are inert to reaction with water.[1,21]

Among the wide range of thin film growth techniques, atomic layer deposition (ALD) has the unique ability to deposit films with Angstrom-level thickness control and perfect conformality in high aspect ratio nanoscale features because of its self-limited growth mechanism.[2,22-25] An ALD process for Pr_2O_3 has been reported using tris(bis(trimethylsilylamido)praseodymium and water.[26,27] This process was not self-limiting in tris(bis(trimethylsilylamido)praseodymium, and the films were contaminated with Si, C, and H impurities. Another ALD process for Pr_2O_3 used tris(*N*,*N'*-diisopropylacetaminidato)praseodymium and water, but did not afford self-limited growth behavior, apparently because of reaction of the Pr_2O_3 layer with additional water to form hydroxides.[1] When tris(tetramethyl-3,5-heptanedionato)praseodymium was used, ozone was required as the co-reactant due to the low reactivity of the β-diketonate ligands with water.[28-30] X-ray diffraction showed that the film was composed of the Pr(IV)-containing phases Pr_6O_{11} and PrO_2, which arise from the strong oxidizing nature of ozone.[30] Moreover, the ALD PrO_x films showed large thickness gradients along the gas flow direction and very rough surfaces.[30] A process employing tris(ethylcyclopentadienyl)praseodymium ($Pr(C_5H_4Et)_3$) and water afforded self-limited growth in both precursors at 130 °C, and gave a growth rate of 0.7 Å/cycle. The resulting Pr_2O_3 films grown on Si had a randomly oriented polycrystalline microstructure.[31] Growth of Pr_2O_3 films was achieved with $Pr(i\text{PrC}_5H_4)_2(i\text{PrNC(Me)N}i\text{Pr})$ and water, with a growth rate of ~1.05 Å/cycle at 200 °C.[32] However, the growth rate increased with increasing pulse length at 200 °C, which was attributed to the hygroscopic nature of Pr_2O_3. The thermogravimetric analysis (TGA) of $Pr(C_5H_4i\text{Pr})_3$ indicated that it is more volatile than $Pr(C_5H_4Et)_3$ and $PrCp_3$.[33] The ALD growth of Pr_2O_3 was reported using $Pr(C_5H_4i\text{Pr})_3$ and ozone at 200 to 250 °C.[33] The growth rate was 0.4 Å/cycle between 200 and 250 °C.[33] Recently, volatile lanthanide complexes containing N,N-dimethylaminodiboranate ligands,[34,35] donor functionalized alkoxide ligands,[36] and

guanidinate ligands[37] have been reported and several were used to deposit selected lanthanide oxides by ALD. However, the deposition of PrO_x films from any of these precursors has not been reported.

$LnAlO_3$ (Ln = La, Pr) films have been grown by ALD using a lanthanide precursor, an Al precursor, and an oxidant.[1,21,38-50] La precursors for $LaAlO_3$ have included La amidinates and formamidinates, $La((NSiMe_3)_2)_3$, $La(thd)_3$, and $La(iPrC_5H_4)_3$. Each of these precursors has limitations, including lack of self-limited growth, impurity incorporation, and variable reactivity toward water. Al precursors were either $AlMe_3$ or $Al(thd)_3$. Processes employing $AlMe_3$ used water as the co-reactant, whereas β-diketonate precursors required ozone. $PrAlO_3$ films have been grown by ALD using $Pr(iPrNCMeNiPr)_3$, $AlMe_3$, and water.[1,21] Because of the lack of self-limited growth in the La or Pr precursors, it is difficult to control the Ln:Al ratio and most films were Al rich.

The exploration of solid phase epitaxy (SPE) of $PrAlO_3$ and other $LnAlO_3$ films grown by ALD on single-crystal $SrTiO_3$ substrates facilitates the discovery of potentially valuable electronic properties, including the 2-dimensional electron gas properties of the resulting heterostructures. SPE requires growth of amorphous films on a crystalline substrate that serves as the nucleation site for the crystallization process. The film crystallization occurs in a second, separate step, following the deposition of the amorphous layer.[51] The low temperatures at which ALD is typically achieved promotes the formation of amorphous $LnAlO_3$ films and make it favorable for the development of SPE processes. However, the lack of self-limited growth in the Ln precursor creates potential issues with controlling the Ln:Al ratios in the $LnAlO_3$ films. Herein, we describe the ALD growth of $PrAlO_3$ films using the precursors $Pr(C_5H_4iPr)_3$, $AlMe_3$,[52] and water (Chart 1). Importantly, self-limited growth occurs with all precursors, and Al-rich $PrAlO_3$ films with Pr:Al ratios of 1.2 to 1.4 are obtained within the ALD window. $PrAlO_3$ films grown on single-crystal

$SrTiO_3$ substrates undergo SPE upon annealing at ~800 °C to yield epitaxial $PrAlO_3$, through a process in which the $SrTiO_3$ layer serves as a template for the crystallization.

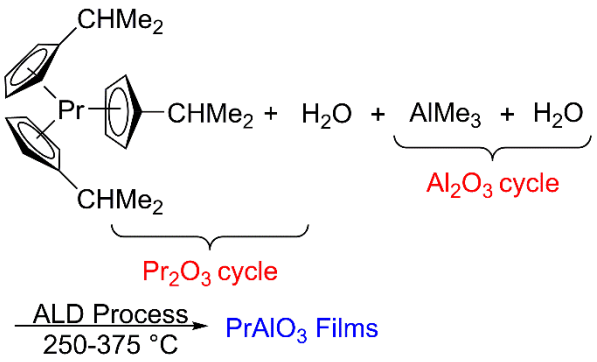

Chart 1. Precursors and chemistry used for the growth of $PrAlO_3$ films.

RESULTS AND DISCUSSION

Pr Precursor Selection. Since $LaAlO_3$ films generally have La:Al ratios of <1, we sought to identify a Pr precursor with Pr_2O_3 growth rate that is as high as possible, to afford close to stoichiometric Pr:Al atomic ratios in a process employing a 1:1 pulsing ratio of the Pr and Al precursors. A Pr_2O_3 ALD process comprising tris(*N*,*N'*-diisopropylacetaminidato)praseodymium and water did not show self-limited growth in the Pr precursor,[1] and amidinate-based precursors were therefore not pursued. The Pr_2O_3 ALD process with $Pr(C_5H_4Et)_3$ and water afforded self-limited growth in both precursors at 130 °C.[31] The Pr_2O_3 growth rate was 0.7 Å/cycle, which is considerably lower than the 1.0 Å/cycle value for Al_2O_3. However, $Pr(C_5H_4Et)_3$ was reported to decompose at 330 °C, which indicates that the compound has very high thermal stability. Early lanthanide cyclopentadienyl complexes with the formula $Ln(C_5H_4R)_3$ (R = H, alkyl) exist as polymeric or oligomeric species in the solid state, with bridging cyclopentadienyl ligands.[53-57] Such aggregated structures should exhibit lower vapor pressures than monomeric species. The inclusion of larger groups on the cyclopentadienyl ligand carbon atoms leads to monomeric

tris(cyclopentadienyl)lanthanide complexes, apparently by steric blocking of bridging carbon atoms.[54] Tris(isopropylcyclopentadienyl)lanthanum ($La(C_5H_4iPr)_3$) was employed as a precursor for the growth of $LaAlO_3$ films, using $AlMe_3$ and water as the other co-reactants.[44] However, the deposition process was not self-limiting in $La(C_5H_4iPr)_3$, the growth rate increased rapidly with precursor dose, and a La/Al pulse ratio of around 5:1 was required to approach 1:1 stoichiometry of La and Al.[44] Since the Pr^{3+} ion is smaller than the La^{3+} ion, we hypothesized that $Pr(C_5H_4iPr)_3$ should be more stable thermally than $La(C_5H_4iPr)_3$ because of better encapsulation of the Pr^{3+} ion. Moreover, the smaller Pr^{3+} ion may enforce a monomeric solid-state structure in the solid and liquid states, which should maximize the volatility of $Pr(C_5H_4iPr)_3$.

$Pr(C_5H_4iPr)_3$ melts at 53-54 °C and thermally decomposes in the liquid state at around 353 °C. The solid-state decomposition temperature of $Pr(C_5H_4iPr)_3$ observed here is higher than that reported previously (250 °C),[33] and is higher than the ~330 °C value reported for $Pr(C_5H_4Et)_3$.[31] The TGA trace conducted under a nitrogen atmosphere showed a single step weight loss (Figure S1), with <10% non-volatile residue at 500 °C, consistent with the earlier report.[33] $Pr(C_5H_4iPr)_3$ is a liquid at the delivery temperature in the ALD reactor (150 °C), which provides a constant vapor pressure to the deposition chamber during the film deposition. A synthesis procedure has been reported for $Pr(C_5H_4iPr)_3$,[58] and the compound is also commercially available. Given the potentially useful precursor properties of $Pr(C_5H_4iPr)_3$, we sought to evaluate it as a precursor in the ALD of $PrAlO_3$ films.

ALD Growth of Pr_2O_3 Films. Pr_2O_3 ALD growth behavior was studied using $Pr(C_5H_4iPr)_3$ and water by varying precursor pulse length, deposition temperature, and number of deposition cycles. The Pr_2O_3 films were grown on Si with a native oxide layer (2–2.5 nm) and on a layer of thermal SiO_2 (90-100 nm thick) on Si. Film thicknesses were determined immediately

after deposition, before possible atmospheric degradation of the Pr_2O_3 layers, using cross sectional scanning electron microscopy (SEM) and ellipsometry, as described in the experimental section. Identical film thicknesses were obtained on both substrates for films grown under the same conditions. Self-limiting deposition using $Pr(C_5H_4iPr)_3$ was assessed at 300 °C using the following pulse sequence for 250 cycles: $Pr(C_5H_4iPr)_3$ (varied), N_2 purge (10.0 s), water (0.1 s), and N_2 purge (10.0 s). $Pr(C_5H_4iPr)_3$ demonstrated saturative growth after pulse lengths greater than 3 s and exhibited a saturative growth rate of 0.85 Å/cycle (Figure 1a). Experiments conducted with 0.2 and 0.3 s pulse lengths of water gave films with very large thickness gradients, consistent with the formation of Pr hydroxides at extended water doses. Even with a 0.1 s water pulse length, a 20-30% thickness gradient was observed across the Pr_2O_3 films that decreased from the direction of the $Pr(C_5H_4iPr)_3$ vapor inlet to the end of the wafer. Such a gradient is almost certainly due to reaction of the Pr_2O_3 layers with water, possibly to afford $Pr(OH)_3$, and is consistent with the well known tendency of lanthanide oxides to react with water to form hydroxides.[1,19-21]

(a)

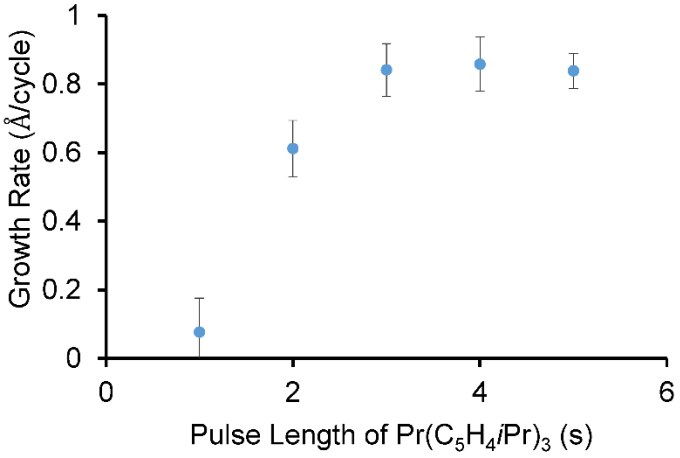

(b)

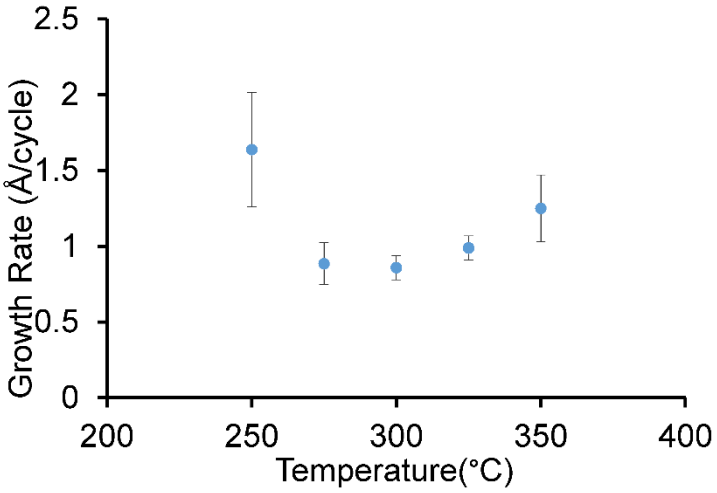

Figure 1. (a) Growth rate of Pr_2O_3 on SiO_2 substrates versus pulse length of $Pr(C_5H_4iPr)_3$ after 250 cycles with a deposition temperature of 300 °C, (b) Growth rate of Pr_2O_3 on SiO_2 substrates versus deposition temperature using $Pr(C_5H_4iPr)_3$ and water after 250 cycles.

The temperature dependence of the Pr_2O_3 growth rate was determined using a saturative pulse sequence of $Pr(C_5H_4iPr)_3$ (4.0 s), N_2 purge (10.0 s), water (0.1 s), and N_2 purge (10.0 s) for 250 cycles (Figure 1b). An ALD window with constant growth rate of 0.85 Å/cycle was observed from 275 to 325 °C and perhaps up to 350 °C. At 250 °C, a higher growth rate was observed, likely because of $Pr(C_5H_4iPr)_3$ condensation. Growth temperatures above 350 °C were not explored, because $Pr(C_5H_4iPr)_3$ decomposes at ~353 °C. The saturative growth rate for this Pr_2O_3 process is considerably higher than the 0.4 Å/cycle growth rate reported for the $Pr(C_5H_4iPr)_3$ and ozone process at 200 to 250 °C.[33]

The Pr_2O_3 thin film growth rate was determined by measuring the film thickness as a function of the number of cycles at 300 °C using the saturative pulse sequence described above for Figure 2 (Figures S2, S3). The resulting plot (Figure S4) was linear, with a slope of 0.77

Å/cycle, which is close to the growth rates determined in Figures 1 and 2. The *y*-intercept was close to zero, indicating the absence of a nucleation delay.

A 21 nm thick film deposited at 300 °C with 250 cycles on a thermal SiO_2 substrate was examined using grazing incidence X-ray diffraction (GI-XRD) immediately after deposition to assess its crystallinity (Figure S5). The diffraction pattern was indexed as Pr_2O_3 (JCPDS 00-006-0410). The reflections were very broad, suggesting nanocrystalline or amorphous material. Infrared spectra of a Pr_2O_3 film on Si with native oxide after 2 and 72 h of air exposure were identical and showed the presence of stretches corresponding to CO_3^{2-} and OH^- groups (Figure S6). Accordingly, the formation of CO_3^{2-} and OH^- groups in the Pr_2O_3 films either occurs during the deposition process (in the case of OH^-) or in <2 h after exposure to air (in the case of CO_3^{2-}).

ALD Growth of $PrAlO_3$ Films. Unlike Pr_2O_3, $LaAlO_3$ and $PrAlO_3$ films are stable toward atmospheric water and CO_2, because of the stability of aluminum oxide layers in the presence of water.[1,19-21] Accordingly, we sought to deposit $PrAlO_3$ films using $Pr(C_5H_4iPr)_3$, $AlMe_3$, and water. $AlMe_3$ and water were selected because they are used in a standard ALD process for the growth of Al_2O_3 films.[52] The comparatively high growth rate of the Pr_2O_3 process outlined above (~0.85 Å/cycle) is significant because it is close to the growth rate of the Al_2O_3 process at 300 °C (~1.0 Å/cycle), thereby possibly maximizing the Pr:Al ratio in the $PrAlO_3$ films. Chart 2 shows an ALD supercycle that was employed to deposit $PrAlO_3$ with a 1:1 Pr:Al precursor pulse ratio. Depositions were conducted on both Si substrates with native oxide and thermal SiO_2 on Si. Similar growth behavior was observed on both substrates, and data for the Si substrates are presented herein. Data for growth on SiO_2 substrates are presented in the supporting information (Figures S7-S17). Self-limited film growth was investigated by examining the dependence of growth rate on the precursor pulse lengths. Saturation was explored using variable pulse lengths of $Pr(C_5H_4iPr)_3$, $AlMe_3$, and

water. The experiments were conducted at 300 °C on Si substrates, with 250 cycles. The pulse lengths of each precursor were varied one at a time, and 10.0 s N_2 purges were used between precursor pulses. As shown in Figure 2, self-limited growth of $PrAlO_3$ films was achieved at 300 °C using a ≥3 s pulse length of $Pr(C_5H_4iPr)_3$, a ≥0.1 s pulse length of $AlMe_3$, and a ≥0.1 s pulse length of water. Importantly, self-limited growth was demonstrated in all three precursors. The growth rate dropped slightly with a 0.3 s pulse length of $AlMe_3$, which may originate from surface poisoning with the very large $AlMe_3$ dose. Alternatively, the large doses of $AlMe_3$ may etch the film surface. $Pr(C_5H_4iPr)_3$ precursor consumption increased with longer pulse lengths (Figure 2a), thereby excluding false saturation because of vapor depletion in the precursor delivery chamber. The consumption of $Pr(C_5H_4iPr)_3$ was measured by weighing the precursor before and after each deposition.

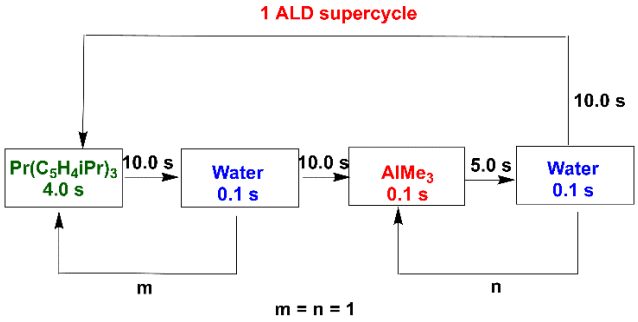

Chart 2. Pulse and purge sequences chart for the deposition of $PrAlO_3$ films.

(a)

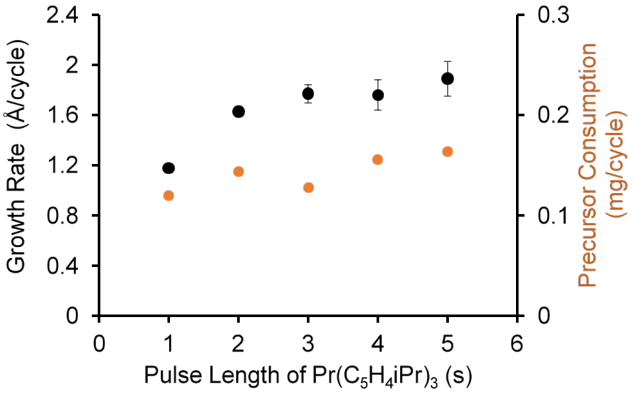

(b)

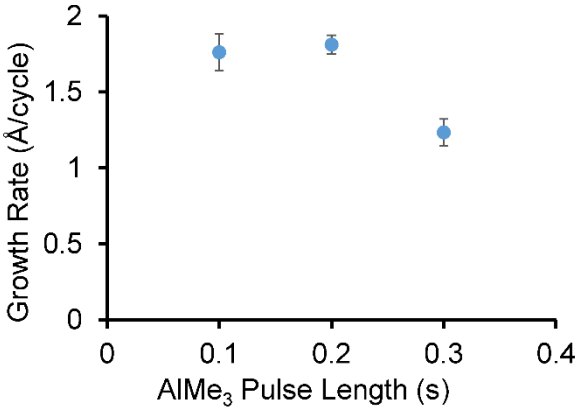

(c)

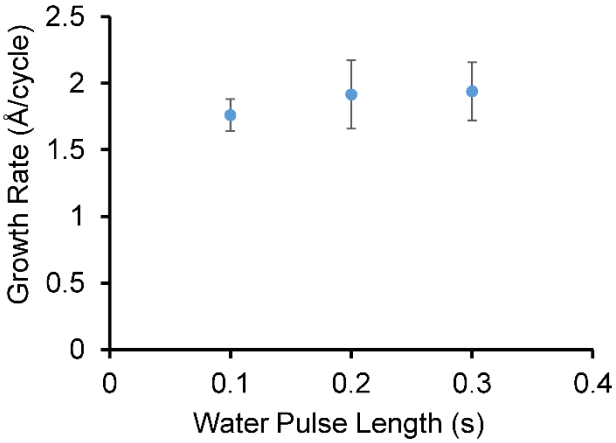

Figure 2. $PrAlO_3$ film growth rate as a function of precursor pulse length for (a) $Pr(C_5H_4iPr)_3$, (b) $AlMe_3$, and (c) water.

Experiments were conducted to explore the temperature dependence of the $PrAlO_3$ film growth (Figure 3a) within the temperature range of 250 to 375 °C. The growth rates varied from a high of 1.72 Å/cycle at 250 and 375 °C, to a low of 1.32 Å/cycle at 350 °C. Intermediate growth rates were observed at 275 and 300 °C (1.60 Å/cycle) and 325 °C (1.48 Å/cycle). A constant growth rate was observed at 275 and 300 °C, and this range may constitute an ALD window. However, the growth rate differences at other temperatures were small. At 375 °C, the growth rate may include contributions from $AlMe_3$[59] or $Pr(C_5H_4iPr)_3$ thermal decomposition, since this temperature is above the decomposition points of both precursors.

(a)

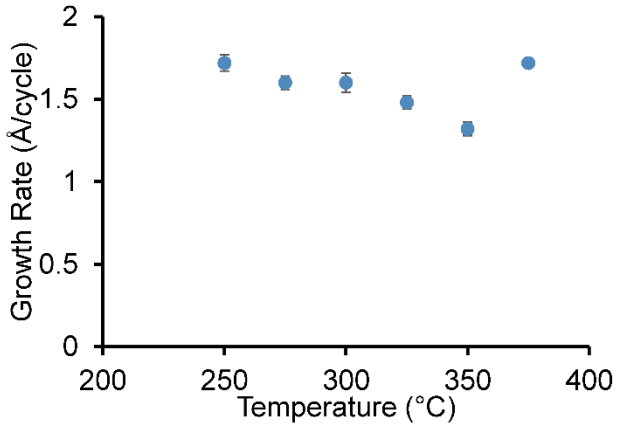

(b)

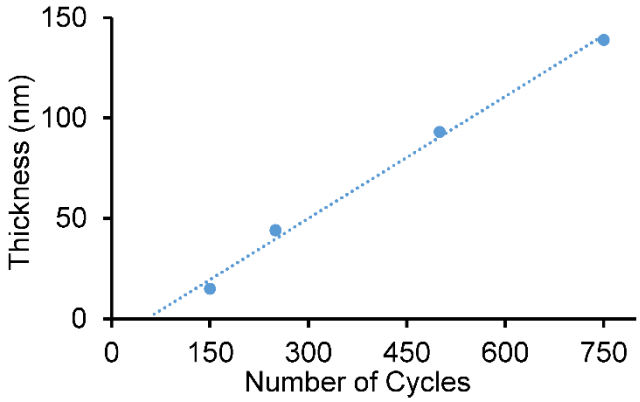

Figure 3. Data for film growth using $Pr(C_5H_4iPr)_3$, $AlMe_3$, and water: (a) Growth rate of $PrAlO_3$ versus deposition temperature with 250 cycles on Si substrates. (b) Thickness versus number of cycles on Si substrates at 300 °C. The line is a linear fit giving a deposition rate of 2.03 Å/cycle and a nucleation delay of about 50 cycles.

A plot of film thickness versus number of cycles is shown in Figure 3b for $PrAlO_3$ films deposited on Si substrates at 300 °C with the saturative pulse sequence described above. A linear increase in the thickness as a function of the number of cycles was observed, with a growth rate of 2.03 Å/cycle. This growth rate is higher than that obtained in Figure 4a within the ALD window. However, the plot in Figure 3b showed a nucleation delay of about 50 cycles, which accounts for the differing growth rates.

Analysis of the $PrAlO_3$ Films. X-ray photoelectron spectroscopy (XPS) measurements were conducted on ~41 nm thick $PrAlO_3$ films deposited on Si and SiO_2 substrates with 250 cycles at 300 °C to determine the purity of the $PrAlO_3$ films and the chemical states of the elements. The XPS analyses showed similar results for the films deposited on both Si and SiO_2. Therefore, only the XPS results for the film grown on Si are shown (Figure 4). Data for the films deposited on SiO_2 substrates are contained in the supporting information (Figures S19-22). Binding energies for the Pr $3d_{5/2}$, Al 2p, and O 1s ionizations were 933.31, 73.25, and 529.38 eV, respectively, and matched well with reported values for Pr_2O_3, Al_2O_3, and oxide ion.[60–63] In the Pr $3d_{5/2}$ plot (Figure 4a), there is an additional ionization centered at ~928 eV, which is attributed to a satellite peak and is a common phenomenon for the Pr $3d_{5/2}$ ionization.[60,61] The XPS depth profile (Figure 4d) shows a uniform distribution of each element throughout the film after removing a few layers of the film surface with argon ion etching. The Pr:Al ratio observed using XPS has a high uncertainty because of the different sensitivities to Pr and Al in the $PrAlO_3$ matrix. Carbon was observed on the film

surface, but, as indicated in Figure 4d, carbon was not observed throughout the film at a level above the detection threshold.

(a)

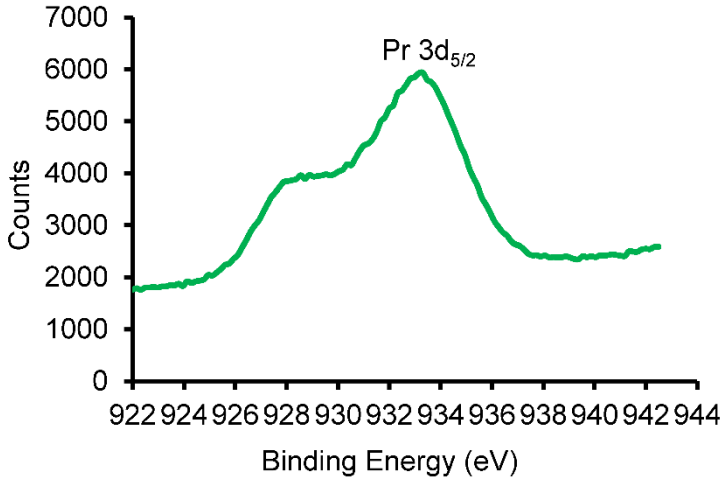

(b)

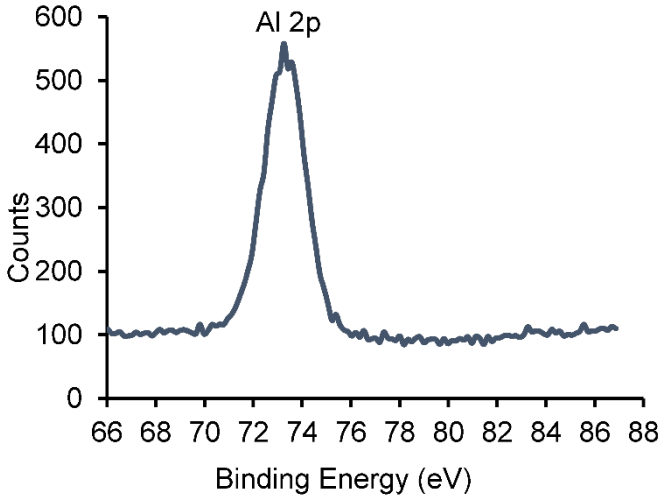

(c)

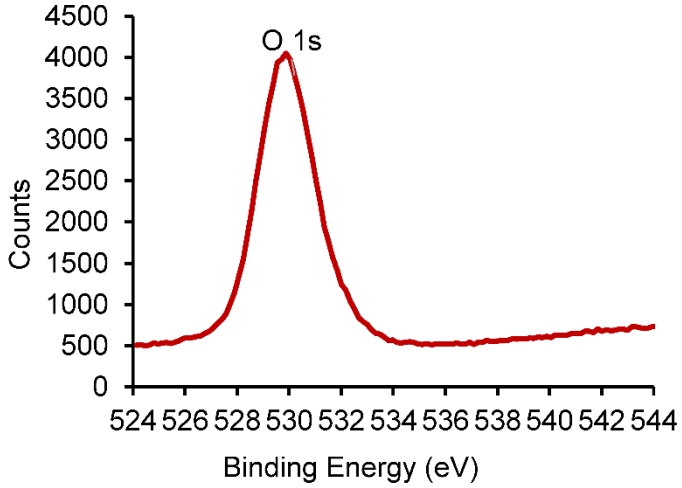

(d)

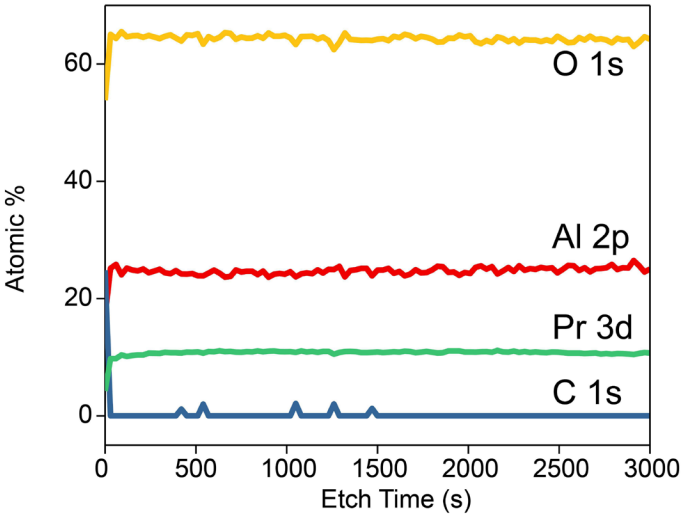

Figure 4. XPS characterization of a 41 nm thick $PrAlO_3$ film deposited on Si at 300 °C. (a) Pr $3d_{5/2}$, (b) Al 2p, (c) O 1s, (d) XPS depth profile of Pr, Al, O, and C atomic concentration during sputter etching of a 41 nm thick $PrAlO_3$ film.

The Pr:Al ratios in the $PrAlO_3$ films were determined more precisely using electron probe microanalysis with X-ray wavelength dispersive spectroscopy (WDS-EPMA). Samples grown at different temperatures within the ALD window with 1:1 Pr:Al precursor pulse ratios were

analyzed, yielding the atomic ratios shown in Table 1. The films are all Al rich, which is consistent with the observed growth rates of the binary oxides Pr_2O_3 (~0.85 Å/cycle) and Al_2O_3 (~1.00 Å/cycle).[52] The calculated Pr:Al atomic ratio based solely upon the growth rate ratio would be 1:1.18, which is Al rich. The growth rate ratio correctly predict that the films are Al rich and give a stoichiometry (~1:1.2) that is similar to those observed by WDS-EMPA. We did not consider density. For the film grown with a 1:1 Pr:Al pulse ratio at 250 °C, the Pr:Al ratio (1:1.70) was higher than other temperatures. At temperatures of 300, 325, 350, and 375 °C, the Pr:Al ratios were approximately constant and ranged from 1:1.23 to 1:1.38. The uncertainty in the WDS-EPMA measurement of the Pr:Al ratio is ~0.02 across this range of compositions, which is far smaller than the differences in composition. A film grown with a 2:1 Pr:Al pulse ratio at 300 °C (Figures S24, S25) afforded a Pr:Al ratio of 1:1.25, which is in the same range as the 1:1 pulse ratios. The origins of the unchanged Pr:Al ratio with the 2:1 pulse ratio are not clear and will require additional experimentation to understand.

Table 1. Pr:Al ratios for the $PrAlO_3$ film deposited on Si at different temperatures using WDS-EPMA. The films were grown with 250 cycles.

Temperature (°C)	Pr:Al precursor pulse ratio	Pr:Al atomic ratio
250	1:1	1:1.70
300	1:1	1:1.33
325	1:1	1:1.38

350	1:1	1:1.26
375	1:1	1:1.23
300	2:1	1:1.25

The Pr:Al ratios obtained by WDS-EPMA differ from those derived from the XPS depth profiling measurements. The absolute composition values obtained using XPS are not as accurate as those obtained from EPMA, since XPS relies on the calibration of elemental sensitivities and can depend on matrix effects. However, the XPS data also indicate that the as-deposited layers are Al-rich, consistent with the WDS-EPMA measurements. More importantly, the XPS depth profiles indicate that there is a constant Pr:Al atomic ratio through the film and low carbon contamination.

Solid Phase Epitaxy of $PrAlO_3$ Films. A 41 nm thick $PrAlO_3$ thin film grown on a Si(100) substrate at 275 °C was characterized by grazing-incidence X-ray scattering. Figure 5a shows the two-dimensional (2D) detector image (covering a 2θ angular range of 13-45°) for a grazing-incidence X-ray scattering of the as-deposited $PrAlO_3$ thin film, in which χ represents the azimuthal angle normal to the 2θ direction. Integrating the 2D detector image along the scattering ring azimuthal angle χ provides measurements of the scattered intensity as a function of 2θ. Figure 5b shows grazing-incidence X-ray scattering patterns acquired from a bare SiO_2/Si substrate and the as-deposited $PrAlO_3$ thin film. The bare Si(100) substrate exhibits a featureless low-intensity background. The X-ray scattering pattern of the as-deposited $PrAlO_3$ includes a broad intensity maximum centered at $2\theta = 30°$, indicating that the $PrAlO_3$ layer is amorphous. A 41 nm thick $PrAlO_3$ film grown on thermal SiO_2 exhibited similar behavior (Figure S18). A 41 nm thick $PrAlO_3$ film deposited on Si with native oxide was annealed at 1000 °C for 8 h. The sample remained

amorphous after this treatment, indicating that the Si substrate does not provide a crystalline template for crystallization.

(a)

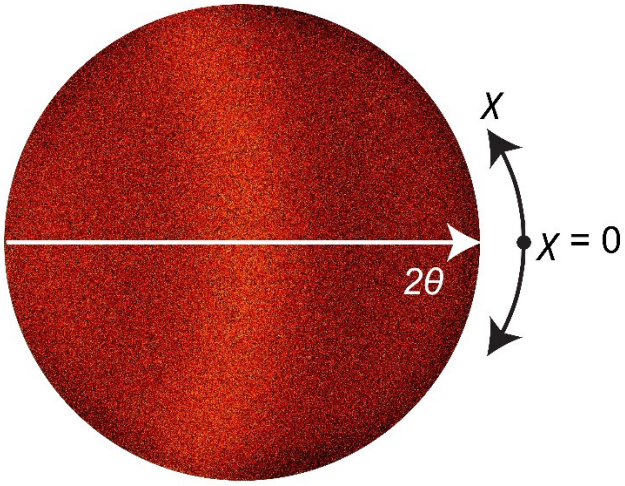

(b)

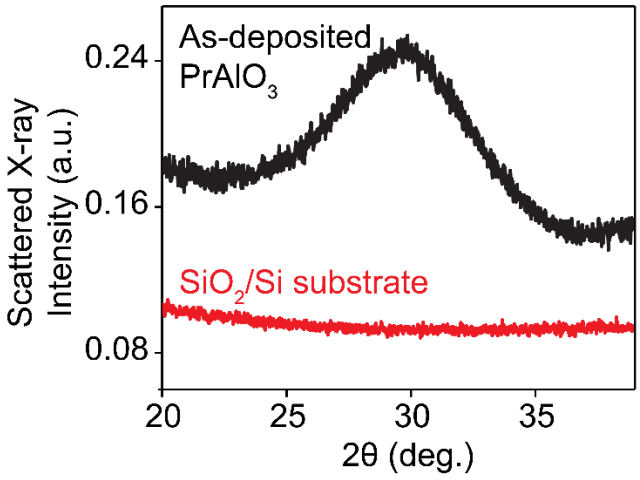

Figure 5. (a) Two-dimensional grazing-incidence X-ray scattering pattern spanning the range of 2θ angles from 13 to 45° for an as-deposited $PrAlO_3$ film on an Si(100) substrate. (b) Azimuthally integrated intensity for $PrAlO_3$ on a Si substrate with native oxide at a deposition temperature of 275 °C (black) and from the native oxide SiO_2/Si substrate without $PrAlO_3$ (red).

X-ray reflectivity (XRR) measurements provided further information about the thickness, roughness, and density of the as-deposited amorphous $PrAlO_3$ thin film. A clear reflectivity signal was obtained from amorphous films because XRR fringes arise from the presence of smooth surfaces and substrate/film interfaces and from the substrate/film electron density contrast but do not require a crystalline thin film. The density of amorphous $PrAlO_3$ was deduced to be 5.2 g cm^{-3} by fitting the XRR data. For comparison, the density of rhombohedral $PrAlO_3$ is 6.73 g/cm^3.[64] Accordingly, the density of the amorphous $PrAlO_3$ film on $SrTiO_3$ is lower than the bulk density. The thickness of the as-deposited amorphous $PrAlO_3$ layer and the surface rms roughness derived a fit of a 42 nm-thick film were 0.6 nm, respectively (Figure S23).

$PrAlO_3$ thin films were deposited on single-crystal (001) $SrTiO_3$ substrates, using the same ALD procedure described above, with a 1:1 Pr:Al pulse ratio (Figure S26). Figure 6a shows grazing-incidence X-ray scattering patterns and detector images of an as-deposited, 206 nm thick $PrAlO_3$ thin film deposited at 300 °C and a bare $SrTiO_3$ substrate. The broad reflection centered at $2\theta = 30°$ indicates that the as-deposited $PrAlO_3$ film is amorphous. The bare $SrTiO_3$ substrate shows a featureless background for comparison. After annealing the amorphous $PrAlO_3$ thin film at 800 °C for 3 h, the structure was characterized by conducting a θ-2θ scan with 10° step size in 2θ. This scan with large steps allows the overall distribution of crystalline phases to be determined. Figure 6b shows the X-ray diffraction from the crystalline $PrAlO_3$ thin film, indicating that the $PrAlO_3$ film is highly (001)-oriented, but does not provide precise information about epitaxy. The strain and orientation distribution are discussed in detail below using a diffraction measurement acquired with smaller angular steps. A small component of grains in other directions are also present in the film, as indicated by the unoriented 110, 111, 210, and 211 reflections apparent in in Figure 6b. The reflections were indexed based on the pseudo-cubic unit cell for $PrAlO_3$ with a

lattice parameter of 3.772 Å.[65] The X-ray diffraction patterns in Figure 6b do not provide any indication that Al_2O_3 has formed during crystallization, suggests that the excess Al atomic concentration is either dissolved in the $PrAlO_3$ or present as small clusters not detected in the diffraction experiment.

(a)

(b)

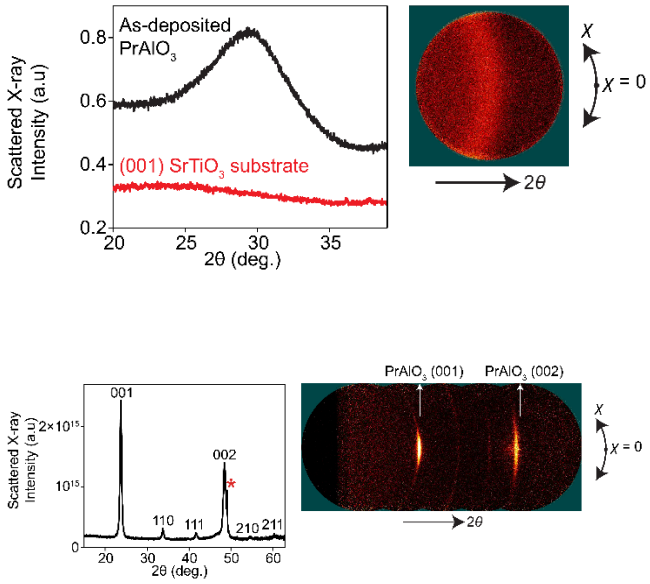

Figure 6. (a) Grazing-incidence X-ray scattering intensity for an as-deposited 206 nm thick $PrAlO_3$ film (black) on a (001) $SrTiO_3$ substrate at a deposition temperature of 300 °C. Scattering intensity from the bare (001) $SrTiO_3$ substrate is shown for comparison. The 2D detector image of the diffraction from the as-deposited amorphous $PrAlO_3$ is shown on the right. (b) X-ray scattering intensity of the $PrAlO_3$ film on (001) $SrTiO_3$ crystallized at 800 °C for 3h. The peak marked with a star is the diffraction from the crystal truncation rod of the $SrTiO_3$ substrate. The right side shows the corresponding 2D detector image.

The epitaxial relationship between the crystallized $PrAlO_3$ film and the (001) $SrTiO_3$ substrate was further examined by conducting a θ-2θ scan with 0.04° step size in 2θ along the Q_z direction of the $SrTiO_3$ substrate, as shown in Figure 7a. The $PrAlO_3$ 00L and $SrTiO_3$ 00L

reflections appear on the same rod of reciprocal space, further indicating that the amorphous $PrAlO_3$ film transforms into an epitaxial layer. The FWHM width of the $PrAlO_3$ (001) reflection rocking curve, shown in Figure 7b, is 7°. The in-plane orientation of the crystallized $PrAlO_3$ layer was probed by measuring the azimuthal angle dependence of the diffracted intensity from the 103 family of $PrAlO_3$ X-ray reflections. The results of this measurement, shown in Figure 7c, indicate that the $PrAlO_3$ layer has four-fold symmetry and that the <100> directions in the $PrAlO_3$ crystal are aligned with <100> directions in the $SrTiO_3$ substrate. The orientation of the $PrAlO_3$ layer is thus epitaxially templated by the $SrTiO_3$ lattice.

(a)

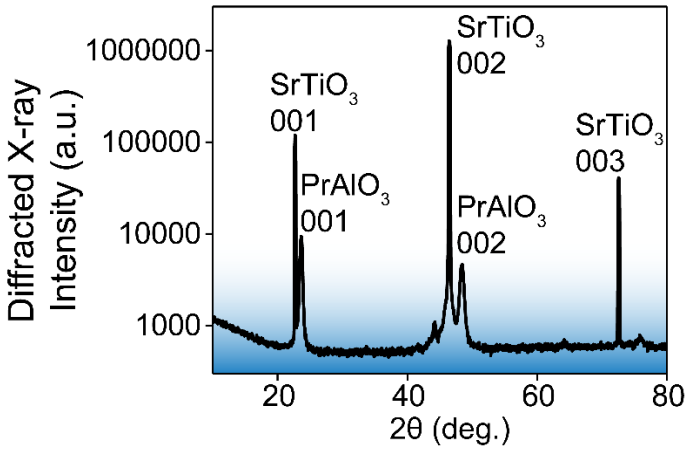

(b)

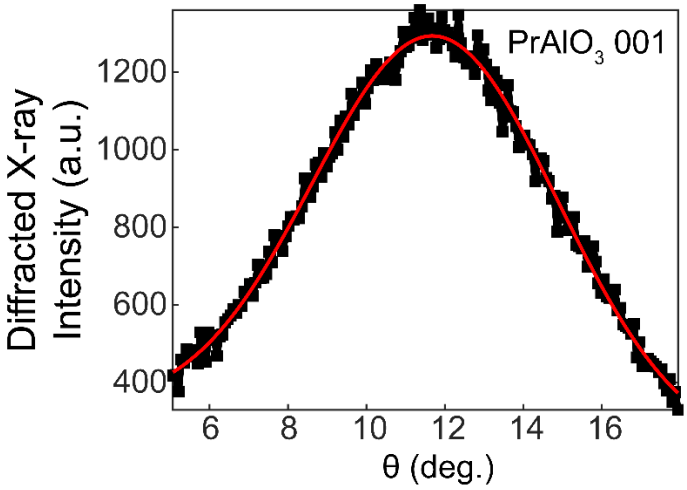

(c)

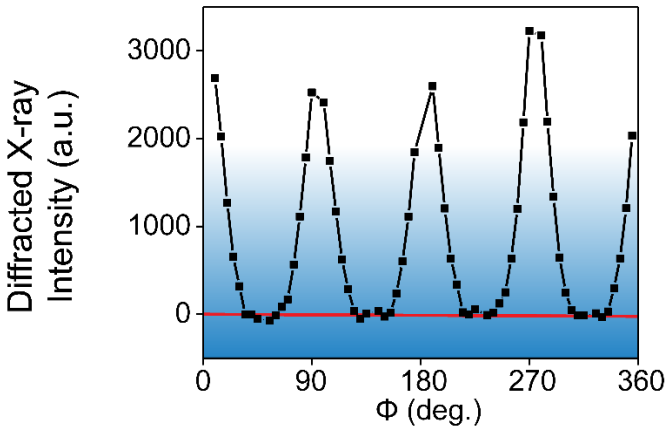

Figure 7. (a) X-ray scattering intensity along Q_z direction and (b) rocking curve scan of $PrAlO_3$ (001) reflection, of the $PrAlO_3$ film on (001) $SrTiO_3$ crystallized at 800 °C for 3h. (c) Azimuthal angle (Φ) dependence of diffracted intensity from 103 reflections of the of the $PrAlO_3$ film on (001) $SrTiO_3$ crystallized at 800 °C for 3h.

The as-deposited $PrAlO_3/SrTiO_3$ interface was characterized using scanning transmission electron microscopy (STEM) with methods described in the supporting information (Figure S27). High-angle annual dark field (HAADF) contrast STEM images revealed that the as-deposited thin films included an interfacial Al_2O_3 layer with a thickness of approximately 5 nm. A series of observations indicate that the interfacial layer crystallizes. Figure 8a shows an HAADF STEM

image of a specimen prepared using focused ion beam lithography. The atomic columns visible in Figure 8a indicate that the Al-rich interfacial layer crystallizes epitaxially in the in the γ-Al_2O_3 phase on the $SrTiO_3$ substrate during the ALD process. A previous ALD study has reported that an as-deposited Al_2O_3 layer formed using $AlMe_3$ and water on $SrTiO_3$ was epitaxial γ-Al_2O_3 crystalline phase when the deposition temperature was ≥300 ºC.[66] γ-Al_2O_3 has a cubic structure with a lattice parameter of 7.911 Å, as shown in Figure 8b.[67,68] The spacings between Al atoms along both [001] and [100] directions of γ-Al_2O_3 are 1.975 Å, which are very close to the atomic spacings of 1.95 Å along both [001] and [100] directions observed for the interfacial layer in Figure 8a. Among the various polymorphic phases of Al_2O_3, only γ-Al_2O_3 has the cubic structure.

(a)

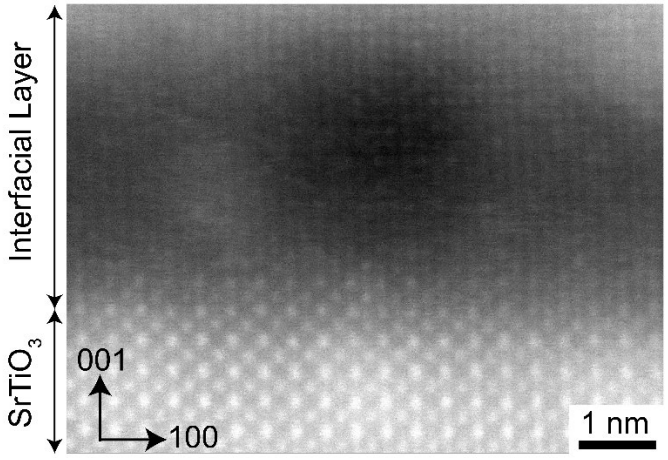

(b)

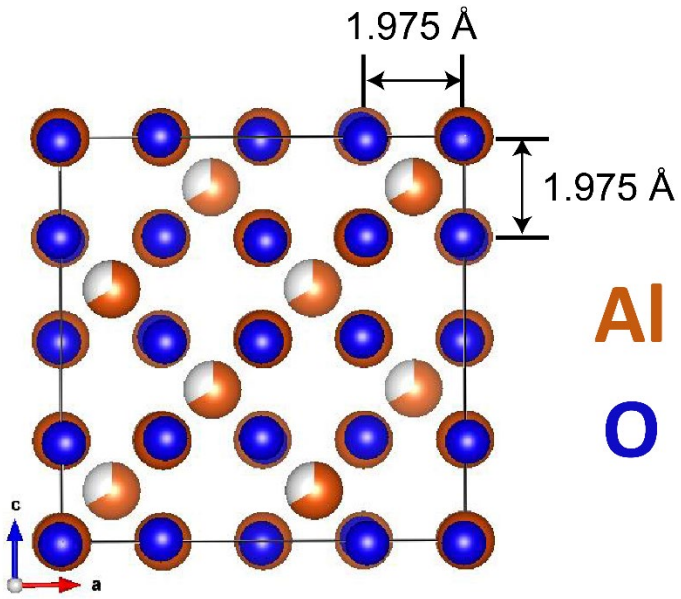

(c)

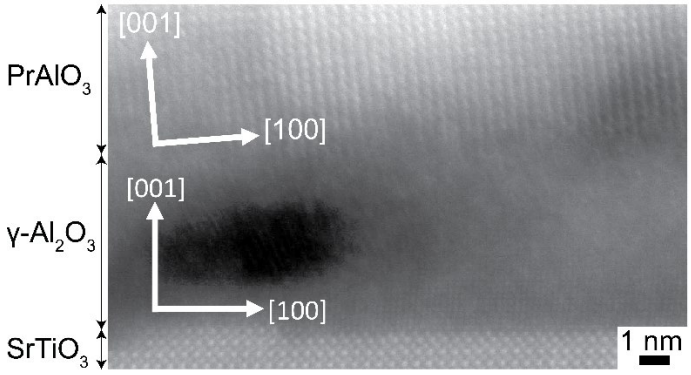

Figure 8. (a) STEM-HAADF image with a high magnification of an as-deposited 206-nm-thick $PrAlO_3$ film grown on (001) $SrTiO_3$ at 300 ºC. (b) Schematic of a unit cell of γ-Al_2O_3 viewed along [010] direction. (c) STEM-HAADF image of a 206-nm-thick film deposited on (001) $SrTiO_3$ and crystallized at 800 ºC for 3 h.

STEM analysis of the film crystallized at 800 ºC for 3 h provides more insight into the epitaxial relationship between the film, the interfacial Al_2O_3 layer, and the substrate. Figure 8c shows a STEM-HAADF image of the 206 nm-thick $PrAlO_3$ film deposited on (001) $SrTiO_3$ and

crystallized at 800 ºC for 3 h. Consistent with the observation in the X-ray diffraction studies, the crystallized $PrAlO_3$ film is highly (001)-oriented. The atomic planes of the $PrAlO_3$ film, the γ-Al_2O_3 layer, and the $SrTiO_3$ substrate appear in the same [010] zone axis, showing the epitaxial relationship is not only along the out-of-plane [001] direction but also along the in-plane [010] direction, which is also consistent with the X-ray observation. The epitaxial relationship of the crystallized sample is actually [001] $PrAlO_3$ // [001] Al_2O_3 // [001] $SrTiO_3$. The misorientation observed in Figure 8c is consistent with the wide mosaic width of the $PrAlO_3$ 001 reflection observed using X-ray diffraction in Figure 7b.

CONCLUSIONS

This study describes the use of $Pr(C_5H_4iPr)_3$, $AlMe_3$, and water as precursors for the growth of nanoscale $PrAlO_3$ films. $PrAlO_3$ thin films have potential applications in advanced transistors and in memory devices.[1-7] Deposition of Pr_2O_3 films was studied first, using $Pr(C_5H_4iPr)_3$ and water. A growth rate of 0.85 Å/cycle was established within an ALD window of 275 to 350 °C, and the resulting films were shown to be crystalline Pr_2O_3 by X-ray diffraction. Importantly, self-limiting growth was demonstrated at 300 °C for $Pr(C_5H_4iPr)_3$. Water pulse lengths of >0.1 s at 300 °C led to films with large thickness gradients, likely because of Pr hydroxide formation upon extended water exposures. $PrAlO_3$ film growth was demonstrated using $Pr(C_5H_4iPr)_3$, $AlMe_3$, and water as the precursors. Self-limited growth was demonstrated in each precursor at 300 °C, and an ALD window was observed from 275 to 325 °C with a growth rate of ~1.7 Å/cycle. The as-deposited films were found to be amorphous using X-ray diffraction and exhibited very smooth surfaces as characterized by XRR. XPS indicated that the layers contained <0.5 at% of carbon impurities. WDS-EMPA analyses indicated that the Pr:Al atomic ratios were 1:1.2 to 1.4 for films deposited with 1:1 $Pr(C_5H_4iPr)_3$:$AlMe_3$ pulse ratios. An amorphous $PrAlO_3$ film grown on Si with

native oxide was annealed at 1000 °C for 8 h. X-ray diffraction demonstrated that the film remained amorphous after this treatment. In comparison, an amorphous $PrAlO_3$ film deposited on (001) $SrTiO_3$ was fully crystallized after annealing at 800 °C for 3 h. The crystallized $PrAlO_3$ film was highly (001) oriented, with a small component of grains in other directions. The $PrAlO_3$ 00L and $SrTiO_3$ 00L reflections appeared on the same rod of reciprocal space, supporting the conversion of amorphous $PrAlO_3$ into an epitaxial layer. The deposition and crystallization of a thin Al_2O_3 layer at the $SrTiO_3$ interface leads will require further refinement of the initial stages of $PrAlO_3$ ALD to form $SrTiO_3/PrAlO_3$ interfaces. The present work demonstrates that the amorphous $PrAlO_3$ on (001) $SrTiO_3$ crystallizes by solid phase epitaxy and adopts the crystal orientation of the $SrTiO_3$ substrate.

EXPERIMENTAL SECTION

$Pr(C_5H_4iPr)_3$ was synthesized according to a literature procedure[58] or purchased from Strem Chemicals. Thermogravimetric analysis of $Pr(C_5H_4iPr)_3$ was performed using a TGA Instrument TGA Q-50 placed inside an argon-filled glove box with a ramp rate of 10 °C/min. The melting point and thermal decomposition temperature measurements for $Pr(C_5H_4iPr)_3$ were determined using an Electrothermal-IA 9000 series melting point apparatus with a heating rate of 10 °C/min. A Picosun R–75 SUNALE ALD reactor was used for the Pr_2O_3 and $PrAlO_3$ thin film depositions. The chamber pressure was maintained at 2 to 4 Torr during depositions. $Pr(C_5H_4iPr)_3$ was delivered at 150 °C in the Picosolid Booster, while $AlMe_3$ and water were delivered at 22 °C using vapor draw bubblers. Ultrahigh purity nitrogen (99.999%, Airgas) was used as carrier gas to deliver the precursors to the deposition chamber. Si(100) with a ~2-2.5 nm native oxide and thermal SiO_2 (90-100 nm) on Si(100) substrates were used for the film deposition without further cleaning. One-side polished single crystal (001) $SrTiO_3$ substrates were cleaned prior to the film

deposition according to a reported protocol.[69] Film deposition temperatures ranged from 250–375 °C. An ALD supercycle (Pr:Al 1:1 pulse ratio) was used to control the Pr:Al ratio in the $PrAlO_3$ films. Film thicknesses were measured using cross-sectional SEM on a JEOL-6510LV scanning electron microscope in a minimum of three different positions in the film. Film thicknesses were additionally determined using ellipsometry on a J. A. Woollam Co. Alpha-SE ellipsometer and with XRR using a Panalytical X'Pert MRD with monochromatic Cu $K\alpha_1$ X-ray radiation at a wavelength of 1.5406 Å. The data were interpreted using the interdiff model of the GenX software package.[70] XRR data were also used to determine surface roughness and mass densities. XPS was performed with a Thermo Scientific Kα XPS spectrometer using a microfocused monochromatic Al Kα X-ray source. The XPS depth profile was performed using an argon ion source to sputter the film. A Cameca SX51 electron microprobe equipped with wavelength dispersive spectroscopy was used to deduce the compositions of the amorphous films. Synthetic $PrPO_4$, which is cataloged as the Smithsonian standard NMNH 168493 (synthesized at Oak Ridge NL by Boatner), was used as the reference standard for the measurement of the amount of Pr element in the deposited films. Al_2O_3 was used as the reference standard for the measurement of the amount of Al and O elements in the deposited films. Si was used as the reference standard for the measurement of Si substrates. As-deposited films were annealed at different temperatures under an oxygen atmosphere for 1–5 h, as described in the text. Crystallinities of the Pr_2O_3 and $PrAlO_3$ films on Si with native oxide and thermal SiO_2 substrates were investigated using X-ray diffraction on a Bruker D8 Advance diffractometer with Cu Kα radiation (λ = 1.5406 Å). X-ray scattering measurements employed a Bruker D8 Advance diffractometer with Cu Kα radiation at a wavelength of 1.54 Å, operating at a tube voltage of 50 kV and current of 1 mA. A 2D area detector subtending an opening angle of 32° was used to record the scattered X-ray intensity. The incident angle of the X-ray beam was

selected based on the beam width and sample size to optimize the amorphous peak signal by maximizing the X-ray footprint on the sample surface. The incident angles for $PrAlO_3$ on $SrTiO_3$ and $PrAlO_3$ on thermal SiO_2 were 2.9° and 3°, respectively. The 2θ angle at the center of the detector was 30° for all measurements. X-ray diffraction along the radial direction of reciprocal space for the $PrAlO_3$ on (001) $SrTiO_3$ sample annealed at 800 °C for 3 h was conducted using a PANalytical Empyrean diffractometer equipped with Cu $K\alpha_1$ radiation (λ = 1.5406 Å). Infrared spectra of thin films were obtained using a Shimadzu FT-IR Tracer 100 spectrophotometer in the transmission mode.

ASSOCIATED CONTENT

Film deposition and characterization data. This material is available free of charge via the Internet at http://pubs.acs.org.

AUTHOR INFORMATION

Corresponding Author

*E-mail: chw@chem.wayne.edu.

Notes

The authors declare no competing financial interest.

ACKNOWLEDGMENT

This research was primarily supported by the U.S. National Science Foundation through the University of Wisconsin Materials Research Science and Engineering Center (DMR-1720415). The authors acknowledge the electron microprobe analysis by Dr. J. H. Fournelle, Department of

Geology and Geophysics, University of Wisconsin-Madison, and funding from the U.S. National Science Foundation Grant No. EAR-1337156 for the purchase of an electron probe micro-analysis instrument. U.S. National Science Foundation Grant Nos. CHE-1427926 and DMR-0922912 are also acknowledged for the purchase of a powder X-ray diffractometer and a field emission SEM, respectively. The authors gratefully acknowledge the use of facilities and instrumentation at the UW-Madison Wisconsin Centers for Nanoscale Technology (wcnt.wisc.edu), which is partially supported by the U.S. National Science Foundation through the University of Wisconsin Materials Research Science and Engineering Center (DMR-1720415).

REFERENCES

(1) de Rouffignac, P.; Gordon, R. G. Atomic Layer Deposition of Praseodymium Aluminum Oxide for Electrical Applications. *Chem. Vap. Deposition* **2006**, *12*, 152–157.

(2) Päiväsaari, J.; Niinistö, J.; Myllymäki, P.; Dezelah, C. L.; Winter, C. H.; Putkonen, M.; Nieminen, M.; Niinistö, L. Atomic Layer Deposition of Rare Earth Oxides. *Top. Appl. Phys.* **2007**, *106*, 15-32.

(3) Leskelä, M.; Ritala, M. Rare-Earth Oxide Thin Films as Gate Oxides in MOSFET Transistors. *J. Solid State Chem*. **2003**, *171*, 170–174.

(4) Robertson, J. High Dielectric Constant Oxides. *Eur. Phys. J. Appl. Phys.* **2004**, *28*, 265–291.

(5) Robertson, J. Interfaces and Defects of High-K Oxides on Silicon. *Solid-State Electron.* **2005**, *49*, 283–293.

(6) Lopes, J. M. J.; Özben, E. D.; Roeckerath, M.; Littmark, U.; Lupták, R.; Lenk, S.; Luysberg, M.; Besmehn, A.; Breuer, U.; Schubert, J.; Mantl, S. Amorphous Ternary Rare-Earth Gate Oxides for Future Integration in MOSFETs. *Microelectron. Eng.* **2009**, *86*, 1646–1649.

(7) Goh, K. H.; Haseeb, A. S. M. A.; Wong, Y. W. Lanthanide Rare Earth Oxide Thin Film as an Alternative Gate Oxide. *Mater. Sci. Semicond. Process*. **2017**, *68*, 302–315.

(8) Ohtomo, A.; Hwang, H. Y. A High Mobility Electron Gas at The $LaAlO_3/SrTiO_3$ Heterointerface. *Nature* **2004**, *427*, 423–426.

(9) Vasylechko, L.; Stepchuck, R.; Prots, Y.; Rosner, H. Concentration and Temperature Induced Phase Transitions in $PrAlO_3$–$SrTiO_3$ System. *Nanoscale Res. Lett.* **2016**, *11*, 17.

(10) Mannhart, J.; Blank, D. H. A.; Hwang, H. Y.; Millis, A. J.; Triscone, J. M. Two-Dimensional Electron Gases at Oxide Interfaces. *MRS Bull.* **2008**, *33*, 1027–1034.

(11) Reyren, N.; Thiel, S.; Caviglia, A. D.; Kourkoutis, L. F.; Hammerl, G.; Richter, C.; Schneider, C. W.; Kopp, T.; Ruetschi, A. S.; Jaccard, D.; Rüetschi1, A. S.; Jaccard, D.; Gabay, M.; Muller, D. A.; Triscone, J.-M.; Mannhart, J. Superconducting Interfaces Between Insulating Oxides. *Science* **2007,** *317*, 1196-1199.

(12) Brinkman, A.; Huijben, M.; Van Zalk, M.; Huijben, J.; Zeitler, U.; Maan, J. C.; Van der Wiel, W. G.; Rijnders, G.; Blank, D. H. A.; Hilgenkamp, H. Magnetic Effects at the Interface Between Non-Magnetic Oxides. *Nature Mater.* **2007,** *6*, 493-496.

(13) Thiel, S.; Hammerl, G.; Schmehl, A.; Schneider, C. W.; Mannhart, J. Tunable Quasi-Two-Dimensional Electron Gases in Oxide Heterostructures. *Science* **2006,** *313* (5795), 1942-1945.

(14) Ariando; Wang, X.; Baskaran, G.; Liu, Z. Q.; Huijben, J.; Yi, J. B.; Annadi, A.; Barman, A. R.; Rusydi, A.; Dhar, S.; Feng, Y.P.; Ding, J.; Hilgenkamp, H.; Venkatesan, T. Electronic Phase Separation at the $LaAlO_3/SrTiO_3$ Interface. *Nature Commun.* **2011,** *2*, 188.

(15) Chambers, S. A. Epitaxial Growth and Properties of Doped Transition Metal and Complex Oxide Films. *Adv. Mater.* **2010**, *22*, 219-248.

(16) Akbashev, A. R.; Chen, G.; Spanier, J. E. A Facile Route for Producing Single-Crystalline Epitaxial Perovskite Oxide Thin Films. *Nano Lett.* **2014**, *14*, 44-49.

(17) Akbashev, A. R.; Falmbigl, M.; Plokhikh, A. V.; Spanier, J. E. In Situ Crystallization Study of Impurity Phases in Bi-Fe-O Thin Films Grown by Atomic Layer Deposition. *CrystEngComm* **2017**, *19*, 166-170.

(18) Evans, P. G.; Chen, Y.; Tilka, J. A.; Babcock, S. E.; Kuech, T. F. Crystallization of Amorphous Complex Oxides: New Geometries and New Compositions Via Solid State Epitaxy. *Curr. Opin. Solid State Mater. Sci.* **2018**, *22*, 229-242.

(19) Mullica, D. F.; Milligan, W. O.; Beall, G. W. Crystal Structures of $Pr(OH)_3$, $Eu(OH)_3$, and $Tm(OH)_3$. *J. Inorg. Nucl. Chem.* **1979**, *41*, 525–532.

(20) Oh, I. K.; Kim, K.; Lee, Z.; Ko, Y. K.; Lee, C.; Lee, J. S.; Myung, M. J.; Lansalot-Matras, C.; Noh, W.; Dussarrat, C.; Kim, H.; Lee, R. H. Hydrophobicity of Rare Earth Oxides Grown by Atomic Layer Deposition. *Chem. Mater.* **2015**, *27*, 148–156.

(21) Lim, S. B.; Rahtu, A.; de Rouffignac, P.; Gordon, R. G. Atomic Layer Deposition of Lanthanum Aluminum Oxide Nano-laminates for Electrical Applications. *Appl. Phys. Lett.* **2004**, *84*, 3957–3959.

(22) Johnson, R. W.; Hultqvist, A.; Bent, S. F. A Brief Review of Atomic Layer Deposition: from Fundamental to Applications. *Mater. Today* **2014**, *17*, 236–246.

(23) George, S. M. Atomic Layer Deposition: An Overview. *Chem. Rev.* **2010**, *110*, 111-131.

(24) Leskelä, M.; Ritala, M. Atomic Layer Deposition Chemistry: Recent Development and Future Challenges. *Angew. Chem. Int. Ed.* **2003**, *42*, 5548–5554.

(25) Leskelä, M.; Ritala, M. Rare-Earth Oxide Thin Films as Gate Oxides in MOSEFT Transistors. *J. Solid State Chem*. **2003**, *171*, 170–174.

(26) Jones, A. C.; Aspinall, H. C.; Chalker, P. R.; Potter, R. J.; Kukli, K.; Rahtu, A.; Ritala, M.; Leskelä, M. Recent Development in the MOCVD and ALD of Rare Earth Oxides and Silicates. *Mater. Sci. Eng., B* **2005**, *118*, 97–104.

(27) Kukli, K.; Ritala, M.; Pilvi, T.; Sajavaara, T.; Leskelä, M.; Jones, A. C.; Aspinall, H. C.; Gilmer, D. C.; Tobin, P. J. Evaluation of Praseodymium Precursor for Atomic Layer Deposition of Oxide Dielectric Films. *Chem. Mater.* **2004**, *16*, 5162–5168.

(28) Päiväsaari, J.; Putkonen, M.; Niinistö, L. A Comparative Study on Lanthanide Oxide Thin Films Grown by Atomic Layer Deposition. *Thin Solid Films* **2005**, *472*, 275–281.

(29) Tiitta, M.; Niinistö, L. Volatile Metal ß-Diketonates: ALE and CVD Precursors for Electroluminescent Device Thin Films. *Chem. Vap. Deposition* **1997**, *3*, 167–182.

(30) Hansen, P.; Fjellvåg, H.; Finstad, T.; Nilsen, O. Structural and Optical Properties of Lanthanide Oxides Grown by Atomic Layer Deposition (Ln = Pr, Nd, Sm, Eu, Tb, Dy, Ho, Er, Tm, Yb). *Dalton Trans.* **2013**, *42*, 10778–10785.

(31) Kondo, H.; Matsui, H.; Furuta, K.; Sakashitha, M.; Zaima, S. Formation of Pr Oxide Films by Atomic Layer Deposition Using $Pr(EtCp)_3$ Precursor. *Jpn. J. Appl. Phys.* **2010**, *49*, 04DA14.

(32) Seppälä, S.; Niinistö, J.; Blanquart, T.; Kaipio, M.; Mizohata, K.; Räisänen, J.; Lansalot-Matras, C.; Noh, W.; Ritala, M.; Leskelä, M. Heteroleptic Cyclopentadienyl-Amidinate Precursors for Atomic Layer Deposition (ALD) of Y, Pr, Gd, and Dy oxide Thin Films. *Chem. Mater*. **2016**, *28*, 5440–5449.

(33) Rao, V. P.; Besancon, B.; Omarjee, V.; Dussarat, C. Development of Lanthanide Precursors as Dopants for Advanced High-k Materials. *ECS Trans.* **2010**, *33*, 145-156.

(34) Daly, S. R.; Kim, D. Y.; Yang, Y.; Abelson, J. R.; Girolami, G. Lanthanide *N,N*-Dimethylaminodiboranates: Highly Volatile Precursors for the Deposition of Lanthanide-Containing Thin Films. *J. Am. Chem. Soc*. **2010**, *132*, 2106–2107.

(35) Daly, S. R.; Kim, D. Y.; Yang, Y.; Girolami, G. Lanthanide *N,N*-Dimethylaminodiboranates as a New Class of Highly Volatile Chemical Vapor Deposition Precursors. *Inorg. Chem*. **2012**, *51*, 7050–7065.

(36) Aspinall, H. C.; Bickley, J. F.; Gaskell, J. M.; Jones, A. C.; Labat, G. Precursors for MOCVD and ALD of Rare Earth Oxides-Complexes of the Early Lanthanides with a Donor-Functionalized Alkoxide Ligand. *Inorg. Chem*. **2007**, *46*, 5852–5860.

(37) Milsanov, A. P.; Fischer, R. A.; Devi, A. Synthesis, Characterization, and Thermal Properties of Homoleptic Rare-Earth Guanidinates: Promising Precursors for MOCVE and ALD of Rare-Earth Oxide Thin Films. *Inorg. Chem.* **2008**, *47*, 11405-11416.

(38) Wiemer, C.; Lamagna, L.; Fanciulli, M. Atomic Layer Deposition of Rare-Earth-Based Binary and Ternary Oxides for Microelectronic Applications. *Semicond. Sci. Technol.* **2012**, *27*, 074103.

(39) Lee, S. W. Two-Dimensional Electron Gas at $SrTiO_3$-Based Oxide Heterostructures via Atomic Layer Deposition. *J. Nanomater.* **2016**, 1671390.

(40) Zhao, L.; Liu, H.-X.; Wang, X.; Fei, Chen, C.-X.; Feng, X.-Y.; Wang, Y.-T. Effects of Annealing Ambient on the Characteristics of $LaAlO_3$ Films Grown by Atomic Layer Deposition. *Nanoscale Res. Lett.* **2017**, 12:108.

(41) Feng, X.-Y.; Liu, H.-X.; Wang, X.; Zhao, L.; Fei, C.-X.; Liu, H.-L. The Study of Electrical Properties for Multilayer La_2O_3/Al_2O_3 Dielectric Stacks and $LaAlO_3$ Dielectric Film Deposited by ALD. *Nanoscale Res. Lett. 2017*, 12:108.

(42) Sønsteby, H. H.; Østreng, E.; Fjellvåg, H.; Nilsen, O. Deposition and X-Ray Characterization of Epitaxial Thin Films of $LaAlO_3$. *Thin Solid Films* **2014**, *550*, 90-94.

(43) Ngo, T. Q.; Posadas, A.; McDaniel, M. D.; Ferrer, D. A.; Bruley, J.; Breslin, C.; Demkov, A. A.; Ekerdt, J. G. Epitaxial Growth of $LaAlO_3$ on $SrTiO_3$-Buffered Si(001) Substrates by Atomic Layer Deposition. *J. Cryst. Growth* **2013**, *363*, 150-157.

(44) Sbrockey, N. M.; Luong, M.; Gallo, E. M.; Sloppy, J. D.; Chen, G.; Winkler, C. R.; Johnson, S. H.; Taheri, M. L.; Tompa, G. S.; Spanier, J. E. $LaAlO_3/SrTiO_3$ Epitaxial Heterostructures by Atomic Layer Deposition. *J. Electron. Mater.* **2012**, *41*, 819-823.

(45) Dong, L.; Liu, Y. Q.; Xu, M.; Colby, R.; Stach, E. A.; Droopad, R.; Gordon, R. G.; Ye, P. D. Atomic-Layer Deposited $LaAlO_3/SrTiO_3$ All Oxide Field-Effect Transistors. *IEDM10* 26.4.1-26.4.4.

(46) Liu, Y.; Kim, H.; Wang, J.-J.; Li, H.; Gordon, R. G. Effects of Low Temperature O_2 Treatment on the Electrical Properties of Amorphous $LaAlO_3$ Films Made by Atomic Layer Deposition. *ECS Trans.* **2008**, *16*, 471-478.

(47) Li, H.; Shenai, D. V.; Pugh, R.; Kim, J. ALD of Lanthanum Aluminate Using Lanthanum Formamidinate Precursor. *MRS Symp. Proc.* **2007**, *1036*, M04-18.

(48) Kukli, K.; Ritala, M.; Pore, V.; Leskelä, M.; Sajavaara, T.; Hegde, R. I.; Gilmer, D. C.; Tobin, P. J.; Jones, A. C.; Aspinall, H. C. Atomic Layer Deposition and Properties of Lanthanum Oxide and Lanthanum-Aluminum Oxide Films. *Chem. Vap. Deposition* **2006**, *12*, 158-164.

(49) Triyoso, D. H.; Hegde, R. I.; Grant, J. M.; Schaeffer, J. K.; Roan, D.; White, B. E., Jr.; Tobin, P. J. Evaluation of Lanthanum Based Gate Dielectrics Deposited by Atomic Layer Deposition. *J. Vac. Sci. Technol. B* **2005**, *23*, 288.

(50) Nieminen, M.; Sajavaara, T.; Rauhala, E.; Putkonen, M.; Niinistö, L. Surface-Controlled Growth of $LaAlO_3$ Thin Films by Atomic Layer Deposition. *J. Mater. Chem.* **2001**, *11*, 2340-2345.

(51) Johnson, B. C.; McCallum, J. C.; Aziz, M. J. *Solid-Phase Epitaxy.* Handbook of Crystal Growth. 2nd Ed. Vol. III, Part A. Thin Films and Epitaxy: Basic Techniques. Kuech, T. F., Ed. Elsevier North-Holland, Boston. 2015. Chap. 7, 317-363.

(52) Puurunen, R. L. Surface Chemistry of Atomic Layer Deposition: A Case Study for the Trimethylaluminum/Water Process. *J. Appl. Phys.* **2005**, 97, 121301.

(53) Baisch, U.; Pagano, S.; Zeuner, M.; Schmedt auf der Gunne, J.; Oeckler, O.; Schnick, W. Synthesis, Structure, and Dynamics of Tris(η^5-cyclopentadienyl)lanthanides and Bis(η^5-cyclopentadienyl)[bis(trimethylsilyl)amido]cerium(III). *Organometallics* **2006**, *25*, 3027-3033.

(54) Stults, S. D.; Andersen, R. A.; Zalkin, A. Structural Studies on Cyclopentadienyl Compounds of Trivalent Cerium: Tetrameric $(MeC_5H_4)_3Ce$ and Monomeric $(Me_3SiC_5H_4)_3Ce$ and $[(Me_3Si)_2C_5H_3]_3Ce$ and Their Coordination Chemistry. *Organometallics* **1990**, *9*, 115-122.

(55) Eggers, S. H.; Kopf, J.; Fischer, R. D. On the Metal Coordination in Base-Free Tris(cyclopentadienyl) Complexes of the Lanthanoids. 2.[1] The X-ray Structure of $(C_5L_5)_3La^{III}$: A Notably Stable Polymer Displaying More Than Three Different La•••C Interactions. *Organometallics* **1986**, *5*, 383-385.

(56) Xie, Z.; Hahn, F. E.; Qian, C. Studies on Organolanthanide Complexes: XXXIX. Synthesis and Molecular Structure of $(MeCp)_3La$ ($MeCp = CH_3C_5H_4$): A Tetrameric Complex of the Type $[(MeCp)_3La]_4$. *J. Organomet. Chem.* **1991**, *414*, C12-C14.

(57) Burns, J. H.; Baldwin, W. H.; Fink, F. H. Crystal Structure of Neodymium Tris(methylcyclopentadienide). *Inorg. Chem.* **1974**, *13*, 1916-1920.

(58) Devyatykh, G. G.; Chernyaev, N. P.; Zverev, Yu. B.; Gavrishchuk, E. M.; Runovskaya, I. V.; Krupnova, E. F.; Chesnokova, S. G. Synthesis and Study of the Saturated Vapor Pressure of Lanthanum, Praseodymium, and Neodymium Tris(isopropylcyclopentadienyls). *Zh. Neorg. Khim.* **1980**, *25*, 2109-2212.

(59) Blakeney, K. J.; Winter, C. H. Thermal Atomic Layer Deposition of Tungsten Carbide Films from WCl_6 and $AlMe_3$. *J. Vac. Sci. Technol. A: Vacuum, Surfaces, and Films* **2018**, *36*, 01A104.

(60) Kruczek, M.; Talik, E.; Pawlak, D. A.; Kolodziejak, K.; Lukasiewicz, T. XPS Study of $PrAlO_3$–$PrA_{11}Al_{18}$ and $PrAlO_3$–Pr_2O_3 Eutectics. *J. Alloys. Compd.* **2007**, *442*, 255–258.

(61) Ryndin, Y. A.; Nogin, Y. N.; Paukshtis, E. A.; Kalinkin, A. L.; Zverev, Y. B. Influence of Pr Ions on the Properties of Pd Supported on Ultra Dispersed Diamond and Graphite from Organometallic Precursors. *J. Mol. Catal.* **1990**, *62*, 45–56.

(62) Sarma, D. D.; Rao, C. N. R. XPS Studies of Oxides of Second- and -Third- Row Transition Metals Including Rare Earths. *J. Electron Spectrosc. Relat. Phenom.* **1980**, *20*, 25–45.

(63) Moulder, J. F.; Stickle, W. F.; Sobol, P. E.; Bomben, K. D. *Handbook of X-ray Photoelectron Spectroscopy*; Perkin-Elmer Corporation; Eden Prarie: MN, 1992; pp 44, 45-55, 56, 144,145.

(64) Geller, S.; Bala, V. B. Crystallographic Studies of Perovskite-Like Compounds. II. Rare Earth Aluminates. *Acta Cryst.* **1956**, *9*, 1019-1025.

(65) Yang, K.; Nazir, S.; Behtash, M.; Cheng, J. High-Throughput Design of Two-Dimensional Electron Gas Systems Based on Polar/Nonpolar Perovskite Oxide Heterostructures. *Sci. Reports* **2016,** *6*, 34667.

(66) Ngo, T. Q.; Goble, N. J.; Posadas, A.; Kormondy, K. J.; Lu, S. R.; McDaniel, M. D.; Jordan-Sweet, J.; Smith, D. J.; Gao, X. P. A.; Demkov, A. A.; Ekerdt, J. G. Quasi-Two-Dimensional Electron Gas at the Interface of Gamma-Al_2O_3/$SrTiO_3$ Heterostructures Grown by Atomic Layer Deposition. *J. Appl. Phys.* **2015**, *118*, 115303.

(67) Zhou, R.-S.; Snyder, R. L. Structures and Transformation Mechanisms of the η, γ, and θ Transition Aluminas. *Acta Crystallogr., Sect. B: Struct. Sci.* **1991**, *47*, 617-630.

(68) Momma, K.; Izumi, F. VESTA 3 for Three-Dimensional Visualization of Crystal, Volumetric and Morphology Data. *J. Appl.Crystallogr.* **2011**, *44*, 1272-1276.

(69) Chen, Y.; Yusuf, H.; Guan, Y.; Jacobson, R. B.; Lagally, M. G.; Babcock, S. E.; Kuech, T. F.; Evans, P. G. Distinct Nucleation and Growth Kinetics of Amorphous $SrTiO_3$ on (001) $SrTiO_3$ and SiO_2/Si: A Step Toward New Architecture. *ACS Appl. Mater. Interfaces* **2017**, *9*, 41304–41042.

(70) Bjorck, M.; Andersson, G. GenX: An Extensible X-Ray Reflectivity Refinement Program Utilizing Differential Evolution. *J. Appl. Crystallogr.* **2007,** *40*, 1174-1178.

TOC GRAPHIC

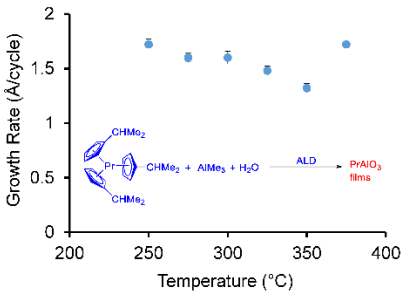
Growth Rate (Å/cycle)
2
1.5
1
0.5
0
200
250
300
350
400
Temperature (°C)
CHMe2
Pr
CHMe2
CHMe2
CHMe2 + AlMe3 + H2O
ALD
PrAlO3
films